Resolving Crystallization Kinetics of GeTe Phase-Change Nanoparticles by Ultrafast Calorimetry

Chen, Bin; de Wal, Dennis; ten Brink, Gert H.; Palasantzas, George; Kooi, Bart J.

Published in:
Crystal Growth & Design

DOI:
10.1021/acs.cgd.7b01498

Publication date:
2018

CRYSTAL GROWTH & DESIGN

Article

Cite This: Cryst. Growth Des. 2018, 18, 1041−1046

pubs.acs.org/crystal

Resolving Crystallization Kinetics of GeTe Phase-Change Nanoparticles by Ultrafast Calorimetry

Bin Chen,* Dennis de Wal, Gert H. ten Brink, George Palasantzas, and Bart J. Kooi*

Zernike Institute for Advanced Materials, Univerisity of Grnoingen, Nijenborgh 4, 9747 AG, Groningen, The Netherlands

Supporting Information

ABSTRACT: Chalcogenide-based phase change materials (PCMs) are promising candidates for the active element in novel electrical nonvolatile memories and have been applied successfully in rewritable optical disks. Nanostructured PCMs are considered as the next generation building blocks for their low power consumption, high storage density, and fast switching speed. Yet their crystallization kinetics at high temperature, the rate-limiting property upon switching, faces great challenges due to the short time and length scales involved. Here we present a facile method to synthesize highly controlled, ligand-free GeTe nanoparticles, an important PCM, with an average diameter under 10 nm. Subsequent crystallization by slow and ultrafast rates allows unravelling of the crystallization kinetics, demonstrating the breakdown of Arrhenius behavior for the crystallization rate and a fragile-to-strong transition in the viscosity as well as the overall crystal growth rate for the as-deposited GeTe nanoparticles. The obtained results pave the way for further development of phase-change memory based on GeTe with sub-lithographic sizes.

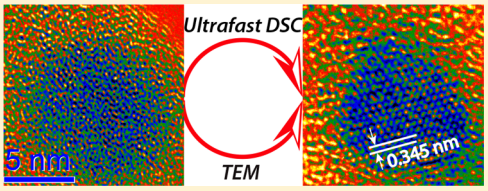

INTRODUCTION

On the basis of the rapid and reversible switching between the amorphous and crystalline phases that offers a strong optical and electrical contrast between these two phases, phase-change materials (PCMs) have attracted attention in various fields, such as optical data storage and novel electrical nonvolatile memories.[1,2] Very recently they were successfully utilized in emerging applications, like solid state displays, on-chip photonic circuitry, and neuromorphic computing.[3−5] The switching of the PCMs relies upon proper heating and cooling of the materials. Heating the amorphous PCMs with pulses (either electric or laser) for tens of nanoseconds triggers the crystallization, and melting followed with quenching them by ultrashort pulses induces the amorphization of the PCMs. Understanding the crystallization kinetics of PCMs thus lies at the heart of their switching. However, owing to the short time scale (tens of nanoseconds) and length scale (~tens of nm) involved, it has been highly challenging for a long time to investigate the crystallization kinetics including the fast switching regime employed in actual memories. However, with the development of ultrafast differential scanning calorimetry (DSC) a powerful tool has become (commercially) available in recent years that enables heating rates up to 40 000 K s^{-1}. Subsequently, the crystallization kinetics of (amorphous) $Ge_2Sb_2Te_5$, AgInSbTe, and GeSb thin films and GeSbTe nanoparticles (NPs) have been investigated by ultrafast DSC.[6−9] As a result, the crystallization behaviors at high heating rates were unraveled as well as the temperature dependency of viscosity and crystal growth rate. Apart from the ultrafast DSC, other techniques were developed to understand the crystallization kinetics of PCMs up to high temperatures, such as laser-based time-resolved reflectivity measurements, isothermal technique monitoring the thickness change of amorphous PCMs and microthermal stage-based resistance measurements.[10−12] Crystal growth rates over wide temperature ranges were unraveled for melt-quenched AgInSbTe and doped-$Ge_2Sb_2Te_5$ PCMs.

GeTe is also a promising candidate for phase-change memory,[13] and it has received considerable attention in particular regarding the understanding of its crystallization kinetics. Dynamic transmission electron microscope (DTEM) was adopted to study the crystal growth rate of GeTe thin films near the melting temperature.[14] Very recently the crystallization kinetics of GeTe thin films was explored by crystallizing flaky powder of the films using ultrafast DSC with a large range of heating rates and subsequent modeling of the obtained results.[15]

Another intriguing property of PCMs is their excellent scalability that is fundamental for future memory devices. Scaling PCMs provides huge advantages,[16−18] such as high information storage density, fast switching speed, and low power consumption per bit. With the continuous down-scaling of phase-change memory, the active volume in phase-change memory is constantly reducing, approaching approximately a thousand nm^3 or even lower, making nanoparticles excellently suited to study the crystallization kinetics of the PCMs. Three dimensional down-scaling of GeTe PCMs into nanoparticles with diameters below 20 nm using chemical synthesis was successfully realized recently.[19,20] In this case, size-dependent polar ordering in crystalline GeTe NPs has been observed.[21] In addition, a strong size dependence of the crystallization temperature has been observed for amorphous GeTe NPs, especially for diameters below 10 nm. For instance, the

Received: October 27, 2017
Published: December 6, 2017

DOI: 10.1021/acs.cgd.7b01498
Cryst. Growth Des. 2018, 18, 1041−1046

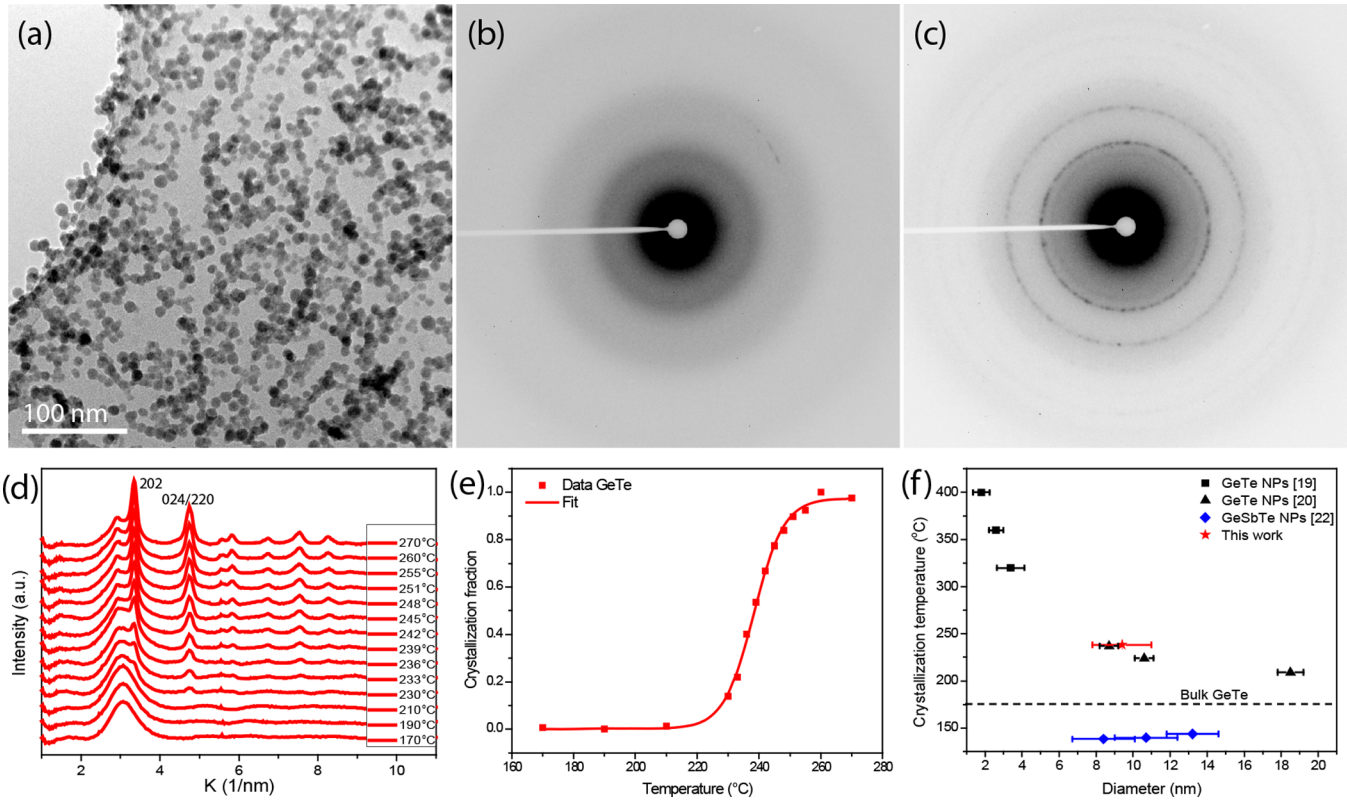

Figure 1. Morphology, crystallinity, and slow crystallization of GeTe NPs. (a) Bright field TEM image showing the morphology of the as-deposited GeTe NPs. Selected area electron diffraction (SAED) patterns of the GeTe NPs recorded at room temperature (b) and 270 °C (c) show the amorphous to crystalline transition. (d) Azimuthal integral of the SAED patterns recorded at different temperatures. The crystallization fraction as a function of temperature is shown in (e), and the size-dependent crystallization temperatures of GeTe and GeSbTe NPs are shown in (f).

crystallization temperature reached 400 °C for GeTe NPs having a diameter of 1.8 nm,[19] which is more than 220 °C higher than the one of bulk GeTe, suggesting ultrahigh stability of the amorphous phase for the NPs.

Despite the successful synthesis of the amorphous and crystalline GeTe NPs, their crystallization kinetics has not been analyzed yet. The focus of the present work is to fill this gap. In contrast to the chemical based syntheses employed in previous works, here we use inert gas condensation based on magnetron sputtering to produce in one-step ligand-free GeTe NPs in an ultrahigh vacuum. The large yield of the deposition allows us to investigate the crystallization kinetics of size controlled GeTe NPs by ultrafast DSC. We present the synthesis of GeTe NPs with excellent size, crystallinity, and composition control by inert gas condensation. Utilizing ultrafast heating (up to 20 000 K s^{-1}) DSC and subsequent numerical modeling allowed us to assess the crystallization kinetics of as-deposited amorphous GeTe NPs in the (extrapolated) temperature range between the glass transition and melting temperatures, providing new insights in the crystallization kinetics of phase-change memory based on nanostructured GeTe.

EXPERIMENTAL METHODS

Sample Preparation. The phase-change GeTe nanoparticles (NPs) were synthesized by magnetron sputtering inert gas condensation using a home-modified nanoparticle deposition system (Nanogen 50). The sample chamber was evacuated to 10^{-8} mbar before NPs deposition. Amorphous GeTe NPs were directly synthesized by sputtering the GeTe target (purity of 99.99%), employing a low current (0.15 A) to avoid the formation of crystalline NPs. The Ar gas flow (purity 99.9999%) used to sputter the target is 35 sccm. A small amount of methane was used to promote the formation of the nascent GeTe clusters in the plasma.[22] Similar to our previous work on GeSbTe NPs,[9] the NPs were deposited directly on a precleaned glass substrate and transmission electron microscope (TEM) holey carbon grids taped outside the periphery of the NPs beam for subsequent characterization of crystallization.

Morphology and Slow Crystallization. The morphology, composition, and slow crystallization of the as-deposited GeTe NPs were characterized by TEM (JEOL 2010) at 200 kV after deposition. The morphology of the GeTe was detected by bright field images, and the crystallinity was characterized by selected area electron diffraction (SAED) patterns. The composition was detected by energy dispersive X-ray spectrometry (EDS) attached to the TEMs (Thermo Instruments on the JEOL 2010 and Bruker Quantax on the JEOL 2010F). The slow crystallization process was determined by *in situ* heating in TEM right after the deposition of the GeTe NPs. Single tilt heating holder (Gatan model 628) with the temperature controlled by a SmartSet Hot Stage controller (Gatan Model 901) was used for heating. The temperature accuracy of the indicator is about 0.1 °C. The SAED patterns probing at the same area were recorded at different temperatures. The temperature interval is 3 °C after the appearance of observable diffraction spots on the SAED patterns. The heating rate above 200 °C is estimated as 0.03 K s^{-1}. During heating, the electron beam was shifted to the copper bar in order to avoid the influence of the electron beam on the crystallization of the NPs.[23] At the end of each temperature step (3 °C), a time interval of 60 s was taken for the sake of stabilization of the TEM membrane to avoid the influence of drifting caused by thermal expansion. The diameter of the selected area aperture for the SAED patterns is 2.5 μm. The NP density is assessed as ~5000 μm^{-2}; however, the total number of NPs selected in the SAED patterns cannot be estimated accurately because of the holes in the carbon support film. The azimuthal integration of the diffraction patterns was performed by the PASAD plug-in (http://

DOI: 10.1021/acs.cgd.7b01498
Cryst. Growth Des. 2018, 18, 1041−1046

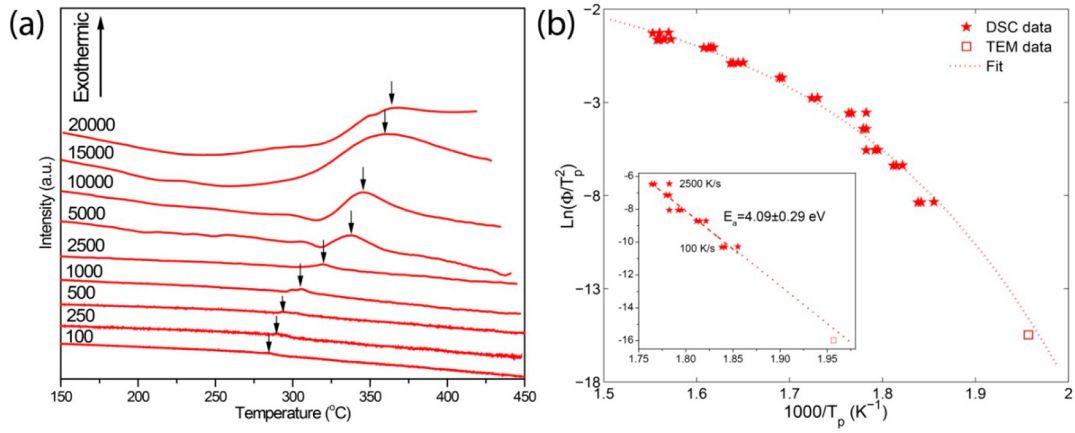

Figure 2. DSC traces for heating rates ranging from 100 to 20000 K s^{-1} (a) and the corresponding Kissinger plot (b). The unit for the heating rate in (a) is K s^{-1}. The inset of (b) demonstrates the zoomed-in Kissinger plot below 2500 K s^{-1}, with the linear fit indicating the activation energy of crystallization. The extrapolation of the linear fit is close to the TEM data point.

www.univie.ac.at/pasad/) in Digital Micrograph software in order to derive the evolution of the diffraction intensity with temperature.[24]

Fast Crystallization and Modeling. The phase transitions of the samples were subsequently measured by ultrafast differential scanning calorimetry (DSC, Mettler-Toledo Flash DSC 1), with the sensor chips (USF-1) each containing the actual sensor and reference area. The GeTe NPs were scraped off from the glass substrate to small pieces, and then a single planar flake consisting of GeTe NPs is positioned parallel to the sensor surface to run the measurements. The approximate size of the flakes is roughly 20 × 20 μm^2. The heating rates (Φ) adopted in this work varied from 100 to 20 000 K s^{-1}. At each Φ, measurements were repeated at least three times for low Φ and 5−10 times for high Φ, as the values of the crystallization temperature become more scattered at high Φ. The thermal lag has no significant influence on the kinetics, as discussed in the Supporting Information. The temperature calibration of the ultrafast DSC was conducted by our early work.[9] Analogous to our previous work,[8,9] the Johnson−Mehl−Avrami−Kolmogrov[25−29] (JMAK) theory was adopted to numerically model the DSC traces at various Φ and fit the crystallization peak temperature to the experimental data. The details of the JMAK calculation can be found in the Supporting Information in our previous work.[8] In the numerical modeling, the generalized MYEGA model was used to describe the temperature dependency of viscosity of the as-deposited amorphous GeTe NPs,[30] as we showed in our previous work that this model describes the experimental data better than MYEGA model.[9] The nucleation process was simplified by a constant nuclei density (site saturation), and the crystallization process is thus largely governed by the temperature dependence of the growth.[6,9] In the fitting process, a data point derived from the *in situ* heating in TEM was also adopted, with the Φ assessed as 0.03 K s^{-1}.

RESULTS AND DISCUSSION

Low Heating Rate Crystallization. The composition, morphology, and crystallinity of the as-deposited GeTe NPs were characterized by TEM. The composition of the GeTe NPs was scrutinized by energy dispersive X-ray spectrometry (EDS), showing the ratio of Ge/Te = 45:55 (±1) at%; see Figure S1 of the Supporting Information. The slight deficiency (~2−3 at) of Ge element is consistent with the results obtained earlier for the GeSbTe and GeTe NPs synthesized by inert gas condensation. The most probable explanation is that the effective sputtering rate of Ge is slightly lower in comparison with Sb and Te. Figure 1a shows the morphology of the as-deposited GeTe NPs, indicating no coalescence of the NPs but only aggregation takes place during deposition. The average diameter of the NPs was then determined as 9.4 ± 1.6 nm, as demonstrated in Figure S2 of the Supporting Information, indicating a relatively narrow size distribution of the GeTe NPs. The selected area electron diffraction (SAED) patterns, as shown in Figure 1b, demonstrate the amorphous nature of the as-deposited GeTe NPs due to the lack of sharp diffraction rings associated with crystal planes.

Analogous to our previous study on GeSbTe NPs, the crystallization of the GeTe NPs at low heating rate was characterized by *in situ* heating in TEM.[22] The GeTe NPs were annealed within the TEM, with the corresponding SAED patterns recorded at each temperature step. Figure 1c illustrates the SAED patterns at 270 °C, with diffraction rings distinctly detectable. Figure 1d demonstrates the azimuthal integral of the SAED patterns, showing that the crystalline peak appears at the temperature ~230 °C and saturated ~260 °C. It is noticeable that the GeTe NPs coalesce during crystallization. This can be distinguished by comparing bright field images of the same area before and after the in situ heating, as shown in Figure S3 of the Supporting Information. The interplanar spacing derived from the SAED patterns are d_{202} = 0.297 nm and $d_{024/220}$ = 0.210 nm, showing excellent agreement with the value for GeTe NPs obtained earlier.[21] The peaks for {024} and {220} planes cannot be resolved for such small NPs. Another work has found that the two peaks merged into one in synchrotron X-ray diffraction for GeTe NPs smaller than 17 nm.[21] Through recording and normalizing the evolution of the diffraction intensity for {024}/{220} peak as a function of temperature, the crystallinity as a function of temperature was then obtained, as shown in Figure 1e. After fitting of the data with the Boltzmann function, the crystallization temperature, defined as the temperature where the maximum first order derivative occurs, is then derived as 238.3 ± 0.3 °C, that is 60 °C higher than that of the bulk GeTe (~175 °C).[31] The fitting was excellent, as assessed by the adjusted R^2 = 0.997. Figure 1f compares the size dependency of crystallization temperature for GeTe and GeSbTe NPs.[19,20,22] Opposite trends for the size dependency can be detected for these two kinds of NPs, where the crystallization temperature drastically rises for GeTe NPs, while a slight decrease is found for GeSbTe NPs when the size of the NPs decrease. Despite the different methods to grow NPs, the data derived for the GeTe NPs in this work agree excellently with the size dependency determined for previous NPs prepared by chemical synthesis. Note that the crystal-

DOI: 10.1021/acs.cgd.7b01498
Cryst. Growth Des. 2018, 18, 1041−1046

lization temperature of GeTe NPs in this work is slightly higher compared to the previous GeTe NPs due to the small amount of methane incorporation to facilitate the formation of nascent NPs during NPs deposition. We have observed in previous work that the methane addition can enhance the stability of the amorphous phase of GeSbTe NPs; therefore a similar effect is expected for GeTe NPs.[22]

Ultrafast Crystallization. The fast crystallization was accomplished by heating single GeTe flakes, that are scraped off from the glass substrate, at various heating rates ranging from 100 to 20 000 K s^{-1} by ultrafast differential scanning calorimetry (DSC). The obtained DSC traces are shown in Figure 2a, where the exothermic crystallization peaks are distinctly observed, as shown by the arrows in Figure 2a. The crystallization peak temperature (T_p) shifts from ~280 °C at 100 K s^{-1} to 365 °C at 20 000 K s^{-1}. Note that, for the GeTe NPs, the crystallization peak was not observed above 20 000 K s^{-1} due to the limit of the maximum temperature that the ultrafast DSC can reach (450 °C). The shift of T_p is expected according to Kissinger:[32]

$$\frac{Q}{R} = -\frac{\mathrm{d}\ln(\Phi/T_p^2)}{\mathrm{d}(1/T_p)} \tag{1}$$

with Q the activation energy for crystallization, R the gas constant, and Φ the heating rate. Then the data obtained by DSC are depicted in a Kissinger plot, as shown in Figure 2b. As shown in the Kissinger plot, the crystallization follows Arrhenius behavior (i.e., a linear dependence in the Kissinger plot) for heating rates Φ below 2500 K s^{-1}, and it breaks down for Φ above 2500 K s^{-1}. The linear fit in the Kissinger plot below 2500 K s^{-1} provides the activation energy for crystallization, E_a = 4.09 ± 0.29 eV. The activation energy is higher compared to the one of the GeSbTe NPs (~2.2 eV).[9] Above 2500 K s^{-1}, the Arrhenius behavior in the Kissinger plot breaks down, generating a strong curvature in the Kissinger plot. Hence, the activation energy of crystallization becomes temperature dependent where it decreases with the increase of temperature.

To understand the break down in the Arrhenius behavior as well as the overall crystallization kinetics, the Johnson–Mehl–Avrami–Kolmogrov (JMAK) theory was adopted to numerically model the crystallization peak temperature at various Φ. In the JMAK modeling, the crystal growth rate is the key factor that dominates the crystallization process. Analogous to our previous work,[8,9] the crystal growth rate between the glass transition and melting temperature is described as

$$U(T) = \frac{4r_{atom}k_BT}{3\pi\lambda^2 R_{hyd}\eta(T)^{\xi}}\left[1 - \exp\left(-\frac{\Delta G(T)}{k_BT}\right)\right] \tag{2}$$

with $U(T)$ the growth rate, r_{atom} the atomic radius (~1.5 Å), λ the diffusional jump distance (~2.99 Å),[33] R_{hyd} the hydrodynamic radius ($R_{hyd} = r_{atom}$), k_B the Boltzmann constant, $\eta(T)$ the temperature dependent viscosity, ξ the decoupling parameter of Stokes–Einstein equation (ξ = 0.65 as used for the GeSbTe NPs[9]), and $\Delta G(T)$ the change of Gibbs free energy, which can be described, according to Thomson and Spaepen, as[34]

$$\Delta G(T) = \frac{\Delta H_m(T_m - T)}{T_m}\left(\frac{2T}{T_m + T}\right) \tag{3}$$

where ΔH_m is the latent heat of melting, approximately 0.186 eV at^{-1}, and T_m is set to 1000 K.[33] In eq 2, the viscosity description is of vital importance in the modeling. As demonstrated by our previous work,[9] the generalized MYEGA model[30] that was originally proposed to describe the viscosity of metallic glass forming liquids outperformed the single fragility MYEGA model to describe the viscosity of as-deposited GeSbTe NPs, because of the relatively clear presence of Arrhenius behavior up to a certain heating rate and only a breakdown of this behavior above this heating rate. Since this is also observed in the present work for a heating rate of 2500 K s^{-1}, it is obvious to adopt the generalized MYEGA model here as well:

$$\log_{10}\eta(T) = \log_{10}\eta(\infty) + \frac{1}{T\left[W_1\exp\left(-\frac{C_1}{T}\right) + W_2\exp\left(-\frac{C_2}{T}\right)\right]} \tag{4}$$

with $\eta(\infty)$ viscosity at infinite temperature (here it is taken as 10^{-3} Pa s), T the temperature, and W_1, C_1, W_2, C_2 the fitting parameters. After the optimization, the modeled T_p at various Φ were depicted as red dotted curve in the Kissinger plot, showing an excellent fitting with the adjusted R^2 = 0.990. The fitting parameters in eq 4 were determined as W_1 = 6184.98, C_1 = 9061.17, W_2 = 4.42 × 10^{-4}, C_2 = 609.17. One can evidently observe that the generalized MYEGA model can nicely fit both the linear (Arrhenius behavior) and the curved (non-Arrhenius behavor) parts in the Kissinger plot.

Viscosity and Fragility. After fitting the data in the Kissinger plot, the viscosity of the as-deposited GeTe NPs is then obtained from eq 4. Figure 3 depicts the temperature dependency of the viscosity of the as-deposited amorphous GeTe NPs. Note that in the generalized MYEGA model, glass transition temperature (T_g) is not directly provided. The T_g is set as the temperature where the viscosity is 10^{12} Pa s, which results in T_g = 467 K for the GeTe NPs. This value for T_g is higher than the one for GeTe film because of the higher

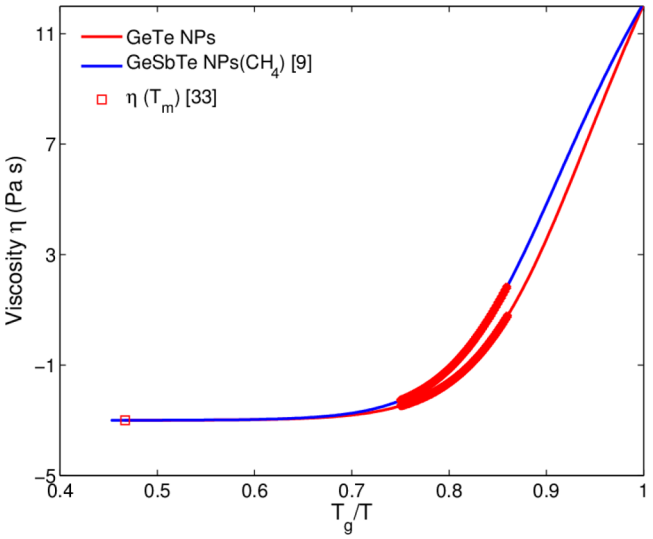

Figure 3. Temperature-dependent viscosity of the GeTe NPs. The high activation energy for the crystallization supports the high fragility. The viscosity at melting temperature, $10^{-3.05}$ Pa s,[33] is also depicted as a red open square for comparison. The thick red marked region indicates the temperature regime accessed by ultrafast DSC.

DOI: 10.1021/acs.cgd.7b01498
Cryst. Growth Des. 2018, 18, 1041−1046

crystallization temperature of the NPs.[33] The fragility, defined as

$$m = \left.\frac{\mathrm{d}(\log_{10}\eta(T)}{\mathrm{d}(T_g/T)}\right|_{T=T_g} \quad (5)$$

was then derived as 78 for the amorphous GeTe NPs from Figure 3. The value for the fragility is lower than that determined for the GeTe thin films (m = 132) owing to the different viscosity models adopted during numerical modeling.[15] However, the fragility of GeTe NPs is higher in comparison with GeSbTe NPs, which is reasonable since GeTe NPs show a higher activation energy for crystallization than GeSbTe NPs (4.09 vs 2.43 eV). For comparison, the viscosity for GeSbTe NPs is also depicted in the Figure 3. The viscosity exhibits a strong (Arrhenius) behavior approaching T_g and becomes fragile (non-Arrhenius) at temperatures above ~1.2 T_g. The extrapolated viscosity fits very well with the value at melting temperature (η = $10^{-3.05}$ Pa s) determined by molecular dynamics simulation.[33]

Crystal Growth Rate. The overall crystal growth rate is one of the most relevant properties of PCMs as it indicates the stability of amorphous phase at relatively low temperatures and the crystallization speed at high temperatures and is thus of key technological importance for applications such as phase-change memory. As illustrated by the solid red curve in Figure 4, the

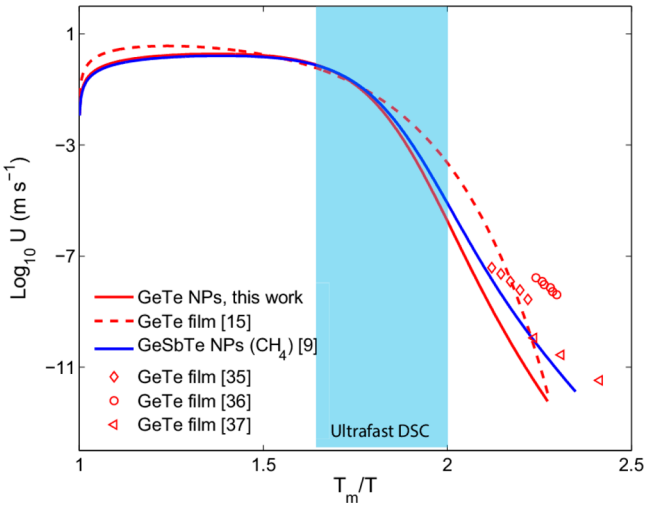

Figure 4. Temperature dependency of crystal growth rate of GeTe NPs. The growth rates for GeTe thin films and GeSbTe NPs are depicted for comparison.

crystal growth rate between T_g and T_m (assuming that T_m is equal to the one for the bulk) is determined by eq 2 for the as-deposited GeTe NPs. For comparison, experimental crystal growth rates at low temperatures for GeTe thin films are shown as well in Figure 4.[35−37] The maximum growth rate (U_m) of GeTe NPs is 1.9 m s^{-1}, occurring at ~720 K (~0.72 T_m), which is slightly higher than GeSbTe NPs (~0.70 T_m) and lower compared to GeTe film (~0.79 T_m).[9,15] The U_m of GeTe NPs is comparable to that of the GeTe thin films (U_m = 3.5 m s^{-1}).[15] However, the GeTe NPs show 2−3 orders of magnitude lower crystal growth rate at temperatures approaching T_g in comparison with the GeTe thin film and the GeSbTe NPs, indicating a higher stability of the amorphous phase of the GeTe NPs. Because of the comparable U_m of GeTe and GeSbTe PCMs, the GeTe NPs are the most favorable for memory applications among the PCMs shown in Figure 4. However, the concern is the melting temperature of the GeTe NPs, which is not accessible by ultrafast DSC. Because of the large increase in the crystallization temperature of the GeTe NPs and well-known decrease in melting temperature during down scaling, the operation window for GeTe NPs can become very small, limiting the applicability of GeTe NPs. For instance the melting temperature of GeTe thin film with a thickness of 2 nm is ~600 °C, 120 °C lower than the bulk value.[31] So further measurements on the size dependence of the melting temperature are required before GeTe NPs can be considered for applications.

CONCLUSIONS

Amorphous GeTe nanoparticles with size, crystallinity, and composition control have been successfully synthesized by inert gas condensation. In-situ heating in a transmission electron microscope reveals that the crystallization temperature of the GeTe NPs at relatively low heating rate is 60 °C higher than the one for bulk GeTe. Ultrafast heating by DSC is then utilized to unravel the crystallization kinetics of the crystallization at higher temperatures. The breakdown of Arrhenius behavior for the crystallization rate is distinctly observed at heating rates above 2500 K s^{-1}. Numerical modeling with realistic description of the viscosity reveals the temperature dependency of the viscosity and crystal growth rate of the GeTe NPs. The high (~2 m/s) maximum crystal growth rate at high temperature (i.e., about 600−800 K) in combination with the very low (~10^{-11} m/s) crystal growth rate when the glass transition temperature (~470 K) is approached implies a promising application perspective of GeTe NPs in memories, but the strongly reducing temperature window between the crystallization temperature and the melting temperature when the NP size reduces can be an obstacle.

ASSOCIATED CONTENT

Supporting Information

The Supporting Information is available free of charge on the ACS Publications website at DOI: 10.1021/acs.cgd.7b01498.

Figures showing the average composition of the GeTe NPs, size distribution, and their morphology before and after heating; details of the thermal lag of the ultrafast DSC (PDF)

AUTHOR INFORMATION

Corresponding Authors

*E-mail: bin.chen@rug.nl (B.C.).
*E-mail: b.j.kooi@rug.nl (B.J.K.).

ORCID

Bin Chen: 0000-0003-1591-0843

Notes

The authors declare no competing financial interest.

ACKNOWLEDGMENTS

We gratefully acknowledge the China Scholarship Council for financial support (of B.C.).

REFERENCES

(1) Wuttig, M.; Yamada, N. *Nat. Mater.* **2007**, *6*, 824−832.

DOI: 10.1021/acs.cgd.7b01498
Cryst. Growth Des. 2018, 18, 1041−1046

(2) Raoux, S.; Welnic, W.; Ielmini, D. *Chem. Rev.* **2010**, *110*, 240−267.
(3) Hosseini, P.; Wright, C. D.; Bhaskaran, H. *Nature* **2014**, *511*, 206−211.
(4) Ríos, C.; Stegmaier, M.; Hosseini, P.; Wang, D.; Scherer, T.; Wright, C. D.; Bhaskaran, H.; Pernice, W. H. P. *Nat. Photonics* **2015**, *9*, 725−732.
(5) Tuma, T.; Pantazi, A.; Le Gallo, M.; Sebastian, A.; Eleftheriou, E. *Nat. Nanotechnol.* **2016**, *11*, 693−699.
(6) Orava, J.; Greer, A. L.; Gholipour, B.; Hewak, D. W.; Smith, C. E. *Nat. Mater.* **2012**, *11*, 279−283.
(7) Orava, J.; Hewak, D. W.; Greer, A. L. *Adv. Funct. Mater.* **2015**, *25*, 4851−4858.
(8) Chen, B.; Momand, J.; Vermeulen, P. A.; Kooi, B. J. *Cryst. Growth Des.* **2016**, *16*, 242−248.
(9) Chen, B.; ten Brink, G. H.; Palasantzas, G.; Kooi, B. J. *J. Phys. Chem. C* **2017**, *121*, 8569−8578.
(10) Salinga, M.; Carria, E.; Kaldenbach, A.; Bornhöfft, M.; Benke, J.; Mayer, J.; Wuttig, M. *Nat. Commun.* **2013**, *4*.10.1038/ncomms3371
(11) Sebastian, A.; Le Gallo, M.; Krebs, D. *Nat. Commun.* **2014**, *5*.
(12) Jeyasingh, R.; Fong, S. W.; Lee, J.; Li, Z.; Chang, K.-W.; Mantegazza, D.; Asheghi, M.; Goodson, K. E.; Wong, H.-S. P. *Nano Lett.* **2014**, *14*, 3419−3426.
(13) Perniola, L.; Sousa, V.; Fantini, A.; Arbaoui, E.; Bastard, A.; Armand, M.; Fargeix, A.; Jahan, C.; Nodin, J. F.; Persico, A.; Blachier, D.; Toffoli, A.; Loubriat, S.; Gourvest, E.; Beneventi, G. B.; Feldis, H.; Maitrejean, S.; Lhostis, S.; Roule, A.; Cueto, O.; Reimbold, G.; Poupinet, L.; Billon, T.; De Salvo, B.; Bensahel, D.; Mazoyer, P.; Annunziata, R.; Zuliani, P.; Boulanger, F. *IEEE Electron Device Lett.* **2010**, *31*, 488−490.
(14) Santala, M. K.; Reed, B. W.; Raoux, S.; Topuria, T.; LaGrange, T.; Campbell, G. H. *Appl. Phys. Lett.* **2013**, *102*, 174105.
(15) Chen, Y.; Wang, G.; Song, L.; Shen, X.; Wang, J.; Huo, J.; Wang, R.; Xu, T.; Dai, S.; Nie, Q. *Cryst. Growth Des.* **2017**, *17*, 3687−3693.
(16) Hirasawa, M.; Orii, T.; Seto, T. *Appl. Phys. Lett.* **2006**, *88*, 093119.
(17) Xiong, F.; Liao, A. D.; Estrada, D.; Pop, E. *Science* **2011**, *332*, 568−570.
(18) Lee, S.-H.; Jung, Y.; Agarwal, R. *Nat. Nanotechnol.* **2007**, *2*, 626−630.
(19) Caldwell, M. A.; Raoux, S.; Wang, R. Y.; Wong, H.-S. P.; Milliron, D. J. *J. Mater. Chem.* **2010**, *20*, 1285−1291.
(20) Arachchige, I. U.; Soriano, R.; Malliakas, C. D.; Ivanov, S. A.; Kanatzidis, M. G. *Adv. Funct. Mater.* **2011**, *21*, 2737−2743.
(21) Polking, M. J.; Urban, J. J.; Milliron, D. J.; Zheng, H.; Chan, E.; Caldwell, M. A.; Raoux, S.; Kisielowski, C. F.; Ager, J. W.; Ramesh, R.; Alivisatos, A. P. *Nano Lett.* **2011**, *11*, 1147−1152.
(22) Chen, B.; ten Brink, G. H.; Palasantzas, G.; Kooi, B. J. *Sci. Rep.* **2016**, *6*.10.1038/srep39546
(23) Kooi, B. J.; Groot, W. M. G.; De Hosson, J. T. M. *J. Appl. Phys.* **2004**, *95*, 924−932.
(24) Gammer, C.; Mangler, C.; Rentenberger, C.; Karnthaler, H. P. *Scr. Mater.* **2010**, *63*, 312−315.
(25) Johnson, W. A.; Mehl, R. F. *Trans. AIME* **1939**, *135*, 396−415.
(26) Avrami, M. *J. Chem. Phys.* **1939**, *7*, 1103−1112.
(27) Avrami, M. *J. Chem. Phys.* **1940**, *8*, 212−224.
(28) Avrami, M. *J. Chem. Phys.* **1941**, *9*, 177−184.
(29) Kolmogorov, A. N. *Bull. Acad. Sci. USSR Math Ser.* **1937**, *1*, 355−359.
(30) Zhang, C.; Hu, L.; Yue, Y.; Mauro, J. C. *J. Chem. Phys.* **2010**, *133*, 014508.
(31) Raoux, S.; Shelby, R. M.; Jordan-Sweet, J.; Munoz, B.; Salinga, M.; Chen, Y.-C.; Shih, Y.-H.; Lai, E.-K.; Lee, M.-H. *Microelectron. Eng.* **2008**, *85*, 2330−2333.
(32) Kissinger, H. E. *Anal. Chem.* **1957**, *29*, 1702−1706.
(33) Sosso, G. C.; Miceli, G.; Caravati, S.; Giberti, F.; Behler, J.; Bernasconi, M. *J. Phys. Chem. Lett.* **2013**, *4*, 4241−4246.
(34) Thompson, C. V.; Spaepen, F. *Acta Metall.* **1979**, *27*, 1855−1859.
(35) Salinga, M.; Kalb, J.; Klein, M.; Sontheimer, T.; Spaepen, F.; Wuttig, M. *EPCOS* **2007**.
(36) Mio, A. M.; Carria, E.; D'Arrigo, G.; Gibilisco, S.; Miritello, M.; Grimaldi, M. G.; Rimini, E. *J. Non-Cryst. Solids* **2011**, *357*, 2197−2201.
(37) Bastard, A.; Bastien, J. C.; Hyot, B.; Lhostis, S.; Mompiou, F.; Bonafos, C.; Servanton, G.; Borowiak, C.; Lorut, F.; Bicais-Lepinay, N.; Toffoli, A.; Sandhya, C.; Fantini, A.; Perniola, L.; Gourvest, E.; Maitrejean, S.; Roule, A.; Sousa, V.; Bensahel, D.; André, B. *Appl. Phys. Lett.* **2011**, *99*, 243103.

DOI: 10.1021/acs.cgd.7b01498
Cryst. Growth Des. 2018, 18, 1041−1046